J Therm Anal Calorim (2012) 108:677–684
DOI 10.1007/s10973-011-2073-9

Examination of the oxidation resistance of Cr–Mo–V tool steel by thermal analysis

D. Chaliampalias · G. Vourlias · E. Pavlidou · K. Chrissafis

MEDICTA2011 Conference Special Chapter

Abstract In the present study, the oxidation behavior of Cr–Mo–V tool steel was examined at different temperatures in air. The examination was conducted by means of thermogravimetric analysis, scanning electron microscopy, and X-ray diffraction (XRD). After non-isothermal oxidation from ambient temperature to 1000 °C, it was revealed that the specimen begins to oxidize over 700 °C, while over 800 °C the oxidation rate increases significantly. Finally over 900 °C, this rate has a considerable value, and the specimen's oxidation resistance is inadequate. From these results, four different oxidation temperatures (805, 835, 865, and 895 °C) were selected for the isothermal test, as referred above, which correspond to different oxidation rates, to determine the oxidation activation energy of the Cr–Mo–V specimens. Energy dispersive X-ray spectroscopy (EDX) and XRD phase identification of the as-formed scales showed that in every case, it contains two distinguishable regions. The inner layer is a mixture of chrome and iron oxides and the outer layer contains iron oxides and is also characterized by high porosity. This phenomenon was explained by the different diffusion coefficients of every element in the steel matrix.

Keywords Steel · Oxidation · Scanning electron microscopy (SEM) · X-ray diffraction (XRD) · Thermogravimetric analysis (TGA)

D. Chaliampalias · G. Vourlias · E. Pavlidou · K. Chrissafis (✉)
Department of Physics, Aristotle University of Thessaloniki, Thessaloniki, Greece
e-mail: hrisafis@physics.auth.gr

Introduction

The wide application of tool steels is attributed to their special mechanical properties that are required in many mechanical devices. Moreover, the oxidation resistance at high temperatures is also required in most of these applications, such as casting and forging dies, blades for hot shearing, and hot extrusion tools [1].

Depending on their chemical contents, tool steels have different oxidation resistances when exposed to high temperatures. The mechanism of their oxidations can be divided into two stages: an initial stage, where the rate of oxidation is linear; and a subsequent stage, where the rate of oxidation follows a parabolic law [2–6]. The first stage includes the adsorption of atomic oxygen on the metal surface, the nucleation of oxides at favorable sites, and the formation of a complete thin film, while during the second stage, the thickness of the initial film increases resulting in the formation of scale [2–8]. Oxidation continues with diffusion through this scale. Depending on the alloy chemical composition and environment, the film may be self-healing from oxidation for a period of time followed by a possible breakdown. Steels with less than 10% chromium, primarily ferritic grades, are limited to work under temperatures below 810 °C. Those containing 10–20% chromium can be used up to 980 °C, whereas steels having chromium content of at least 25%, can be used up to 1090 °C [8].

The Cr–Mo–V (Calmax) series of tool steels are developed as a possible alternative to the high-speed steels and are used in manufacturing cutting tools. Their nominal chemical composition is C: 0.60 wt%, Si: 0.35 wt%, Mn: 0.80 wt%, Cr: 4.50 wt%, Mo: 0.50 wt%, V: 0.50 wt%, and Fe: balance. Its microstructure contains chromium carbides, as a result of eutectic phase transformations during

solidification and during the tempering procedure of the tool steel at the formation process, which promote the microhardness and the wear resistance.

The present study represents a combined study of reaction kinetics and characterization of the oxides formed during high-temperature oxidation of Calmax tool steel. More specifically, kinetics is used for the evaluation of the growth of the scale, and as a result, data could be mined for the evaluation of the oxidation rate constants under the conditions of the experiments and also significant information is gathered regarding the durability of the examined material when exposed in similar aggressive environments.

Experimental

The specimens, which were used, were cut from a Cr–Mo–V steel sheet. In particular, the experimental coupons were machined in rectangular specimens with dimensions 5 × 3 × 2 mm, while their surfaces were very well polished up to 5 μm with alumina emulsion. Their oxidation took place in a Setaram TG-DTA Setsys 16/18 system, in which the specimens were placed in alumina crucibles together with an empty one which was used as reference. The specimens were heated from ambient temperature up to 1000 °C with a heating rate of 10 °C min^{-1} in a 50 mL min^{-1} flow of air. During isothermal oxidations, the specimens were oxidized in flowing air at 805, 835, 865, and 895 °C for 20 h. Continuous records of the specimen temperature and mass were taken to allow a quantitative estimation of oxidation and the on-line monitoring of the oxidation phenomena.

The microstructure and the chemical composition of the tool steel before and after oxidation were determined by combining the results of two analytic procedures. The first one was scanning electron microscopy (SEM) using a 20 kV JEOL 840A SEM equipped with an OXFORD INCA 300 energy dispersive X-ray analyzer (EDX) (detection limit 0.2 wt% under ideal conditions) and the necessary software to perform point microanalysis, linear microanalysis, and chemical mapping of the surface under examination. The second one, for the phase identification, was X-ray diffraction (XRD) analysis using a 2-cycles Rigaku Ultima+ diffractometer (40 kV, 30 mA, Cu Kα radiation) with Bragg-Brentano geometry (detection limit 2% approximately).

Results and Discussion

In order to retrieve representative results concerning the chemical content of the tool steel, several areas of the surface were analytically studied. It was found that in every case, the surface consisted of a ferrous matrix in which numerous dark- and light-colored islands were formed (Fig. 1a). This is attributed to the existence of the strongly carbide-forming elements C, Mo, and V, which leads to the formation of finely dispersed spherical carbides. Thus, the Cr–Mo–V tool steels have higher values of microhardness, with nominal value of 200 HB [9], than common steels.

EDX elemental analysis on those areas revealed that the dark-colored agglomerations (area #1) consist of 44 wt% Fe, 1 wt% C, 48 wt% Cr, and 7 wt% V, and correspond to a mixture of Cr and V carbides. The existence of agglomerations promotes the durability of the material and its wear resistance. In addition, they hinder the growth of large size grains, which also contributes to further enhancement of the microhardness [1]. The common matrix areas (area #2) consist of 94.5 wt% Fe 0.8 wt% C, 4.5 wt% Cr, and 0.2 wt% V and correspond to the nominal composition of Calmax tool steel. Diversifications regarding the nominal composition of Calmax steel (such as the V composition) are attributed to the relevant uncertain nature

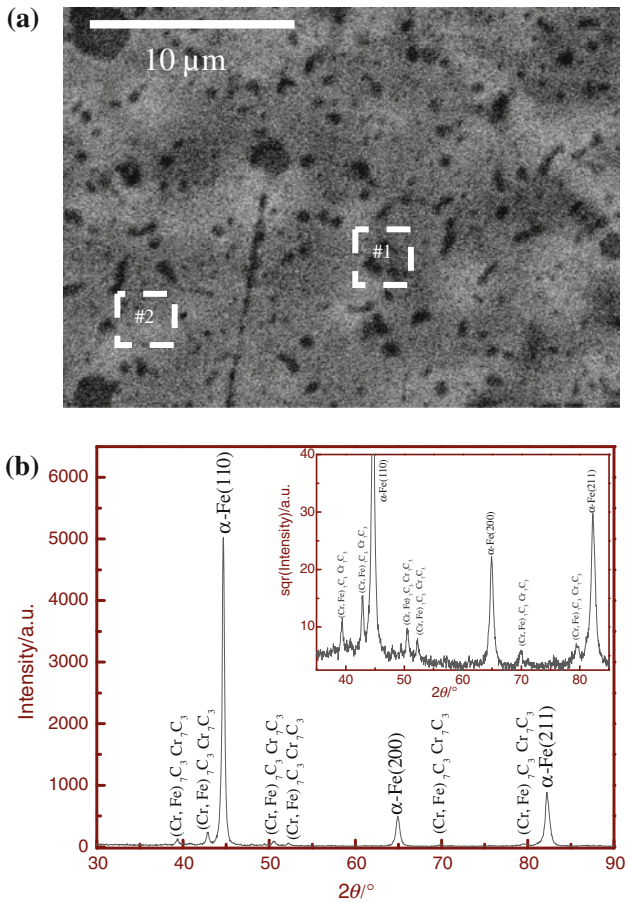

Fig. 1 **a** Plane view SEM micrograph of Cr–Mo–V tool steel. Areas denoted as #1 correspond to Cr and V carbides, while areas denoted as #2 are matrix areas. **b** The corresponding XRD pattern. The indexing of the peaks was accomplished with the following PDF cards: α(Fe): 65-4899, Cr_7C_3: 11-0550, $(Cr,Fe)_7C_3$: 05-0720 [10]

of low content values which are near the measurement limit of the EDX analyzer. The compositions of the remaining elements iare not presented as their contents are below the measurement limit of the instrument.

The corresponding XRD diffraction pattern was identified as shown in Fig. 1b to reveal the phases appearing in the Cr–Mo–V alloy. The presence of Cr_7C_3 and $(Cr,Fe)_7C_3$ carbide peaks were traced, beyond the main peaks corresponding to α-ferrite [10]. The identification of the particular carbides is in agreement with previously published studies on similar tool steels [11–13]. The exact vanadium carbides were not possible to be identified through XRD, as they were not present in the diffraction pattern because of their untraceable low content on the surface of the material. The same pattern is given in the inset graph with the square root of the intensity on the y-axis, to better present the Cr carbide peaks.

In order to examine the oxidation resistance of the Cr–Mo–V tool steel under non-isothermal conditions, thermogravimetric experiments were performed in air environment by heating the coupons from room temperature up to 1000 °C. By this way, from the as-received mass gain graph, the critical temperatures were defined at which the oxidation rate changes significantly. The mass gain per unit area versus temperature for the particular tool steel is presented in Fig. 2.

From this graph, it is revealed that Cr–Mo–V tool steel does not oxidize, significantly, up to 750 °C. Above 800 °C, the mass gain of the specimen increases, and from ≥850 °C, the oxidation rate is relatively high.

The as-oxidized specimen, was examined with SEM microscopy to observe the final state of their surface after the exposure. The cross-sectional examination (Fig. 3a) revealed that a thick oxide layer is formed over the surface of the tool steel. The extreme oxidation conditions at temperature where the oxidation rate is high resulted in the delamination of a significant part of the as-formed oxide because of the thermal expansion coefficient mismatch between the different types of iron oxides formed in the scale [14]. This was also experimentally proved as several oxide pieces were found detached in the oxidation ceramic crucible. Thus, the thickness of the scale may be bigger than the one which is demonstrated in Fig. 3a.

Chemical analysis of the as-formed scale showed that it contains two regions. The layer in contact with the non-oxidized tool steel has average 6-μm thickness and contains a mixture of chrome (37 wt%), iron (43 wt%), oxygen (17 wt%), and significant vanadium (3 wt%) amounts. The upper layer, has an average thickness of 8 μm and consists only of iron (81 wt%) and oxygen (19 wt%) elements.

The identification of the corresponding XRD diffraction pattern (Fig. 3b) revealed that the surface of the specimen consists, only, of hematite (Fe_2O_3) and magnetite (Fe_3O_4). No chrome-containing compounds were detected in the XRD diffraction because the X-rays were totally absorbed

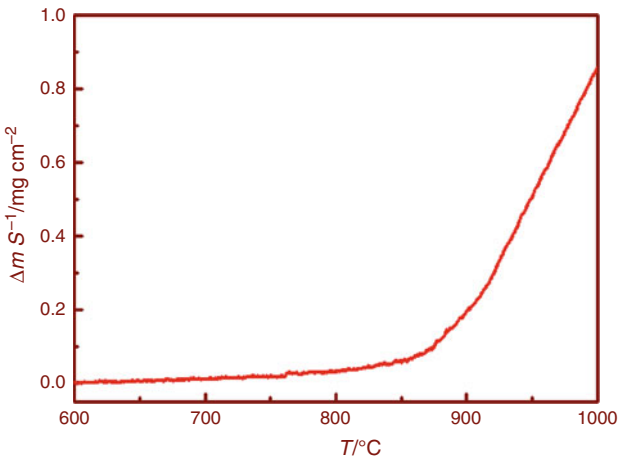

Fig. 2 Mass gain per unit area ($\Delta m/S$) as a function of temperature with heating rate 10 °C min^{-1} of the specimens

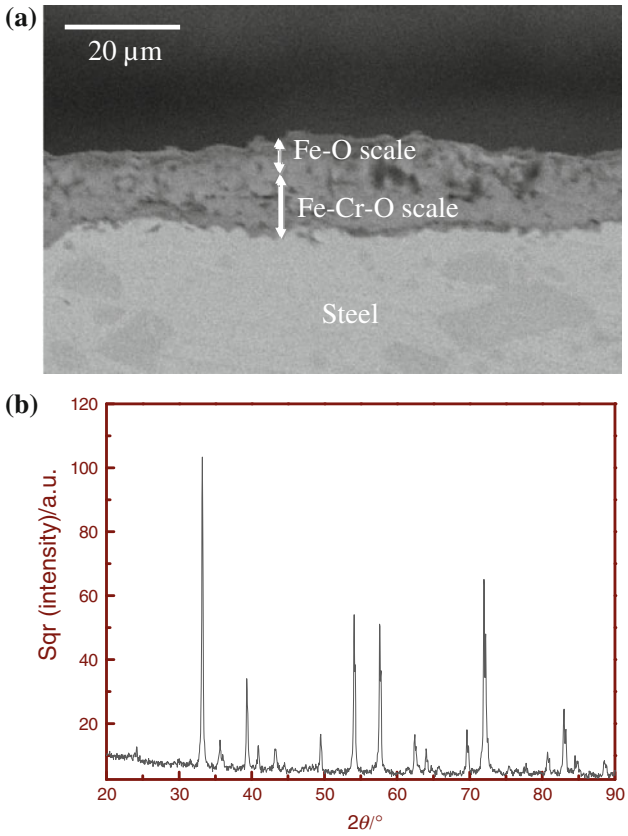

Fig. 3 **a** Cross-sectional SEM micrographs of the Cr–Mo–V tool steel after non-isothermal oxidation (**a**) and the corresponding XRD pattern (**b**). The indexing of the peaks was accomplished with the PDF cards: 87-1166, 85-0987 (Fe_2O_3)

by the Fe oxides and could not capture the lower Cr-containing layer that was beyond their reach .

In order to examine the oxidation resistance of the tool steel in detail, several isothermal oxidation experiments were performed and the mass change was measured at constant exposure time. The mass gain per surface unit ($\Delta m/S$) is a function of the exposure time t in aggressive environments, and the remaining factors affecting the phenomenon are incorporated in a rate constant k_p. Therefore, the determination of the function of $\left(\frac{\Delta m}{S}\right)^2$ versus t, along with the calculation of the constant k_p is an effective way of estimating accurately the oxidation resistance of the specimens. For the oxidation of a metallic material, it may be assumed that kinetics obey a parabolic law [2, 4, 7]. Hence, the mass gain per unit area can be expressed as

$$\left(\frac{\Delta m}{S}\right)^2 = k_p t \tag{1}$$

where $\frac{\Delta m}{S}$ is the mass gain per surface unit at time t, and k_p is the rate constant. In order to better describe the high-temperature scaling kinetics, a plot $\left(\frac{\Delta m}{S}\right)$ versus $t^{0.5}$ is inherently superior to the $\left(\frac{\Delta m}{S}\right)^2$ versus t, for the determination of the parabolic rate constant [15–17].

For the isothermal oxidation tests, four different oxidation temperatures were selected to evaluate the oxidation resistance of the Cr–Mo–V tool steels. The duration of the oxidation test was in every case 20 h. The first isothermal oxidation was performed at 805 °C which is the starting temperature of oxidation according to the non-isothermal TG measurements. It is, however, probable that the oxidation starting temperature be lower, considering the decarburization effect realized at this temperature range, which results in a fairly appreciable decrease of the mass gain and compensates the mass gain increase because of oxidation, and for this reason, it is not observed in the corresponding curve of Fig. 2. The other temperatures were 835 and 865 °C which correspond to intermediate oxidation temperatures. Finally, the highest oxidation temperature was 895 °C at which the oxidation rate is high.

The results of the isothermal study are summarized in the plots of Fig. 4. There is a characteristic similarity between the different curves. Oxidation seems to be impeded with exposure time, and this means that the scale is rather protective and its growth decreases the rate of its development.

Figure 5 presents the same graph using the correlations Δm^2 versus t and Δm versus $t^{0.5}$ from the thermogravimetric measurements received at 805 °C (a) and 895 °C (b). From this graph, it is concluded that the development of the oxidation can be described with a straight line with low uncertainty for medium exposure times. However, at

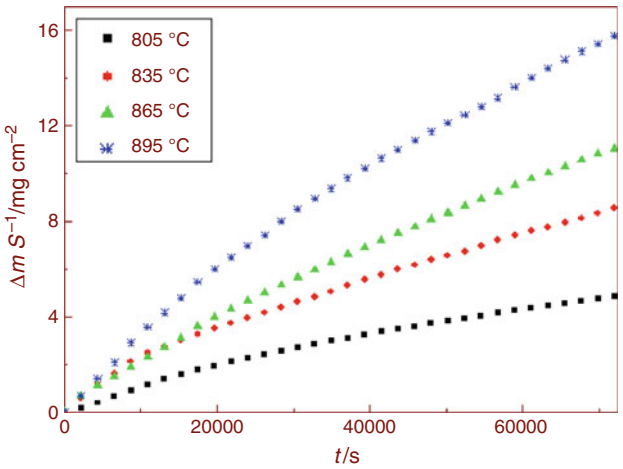

Fig. 4 Evolution of the mass gain per unit area ($\Delta m/S$) as a function of the oxidation time (t) for four different isothermal temperatures (805, 835, 865, and 895 °C)

low exposure times, the phenomenon is not linear because initially a transient oxidation phenomenon takes place, which finally results in the formation of a passivating stable scale. After the formation of this oxide layer, the oxidation process develops by the diffusion of the ions through the scale, and hence the mass change rate becomes parabolic. The same conclusions are, also, drawn when the plot of Δm versus $t^{0.5}$ is used in graphs of Figs. 5c and 7d [15, 17].

From the plots of Fig. 5, the values of the rate constant k_p were calculated only from the linear part of each curve. In every case, the results reveal the function between the mass gain and time is parabolic. As a result, the rate constant increases as the oxidation temperature increases. The results of the oxidation kinetics examination are summarized in Table 1.

For the calculation of the activation energy the Arrhenius law can also be used:

$$k_p = k_o \exp(-E/RT) \tag{2}$$

where k_o is the pre-exponential factor, E is the activation energy, R is the gas constant, and T is the absolute temperature.

The activation energy E was calculated from the curves of the logarithm of k_p versus $1000/T$ for the k_p values from Eq. 2 ($\ln k_p = \ln k_o - E/RT$), using the correlations Δm^2 versus t (Fig. 6a) and Δm versus $t^{0.5}$ (Fig. 6b). The results reveal that both the activation energies as calculated from both graphs have approximately the same value (Table 2) and is equal to 269 kJ mol^{-1}.

In Fig. 7, the cross-sectional micrographs of the oxidized specimens are presented. The thickness of the as-formed scale was measured in several areas, and it was found to be increasing with the oxidation temperature. This is a reasonable effect of the oxidation temperature, as the

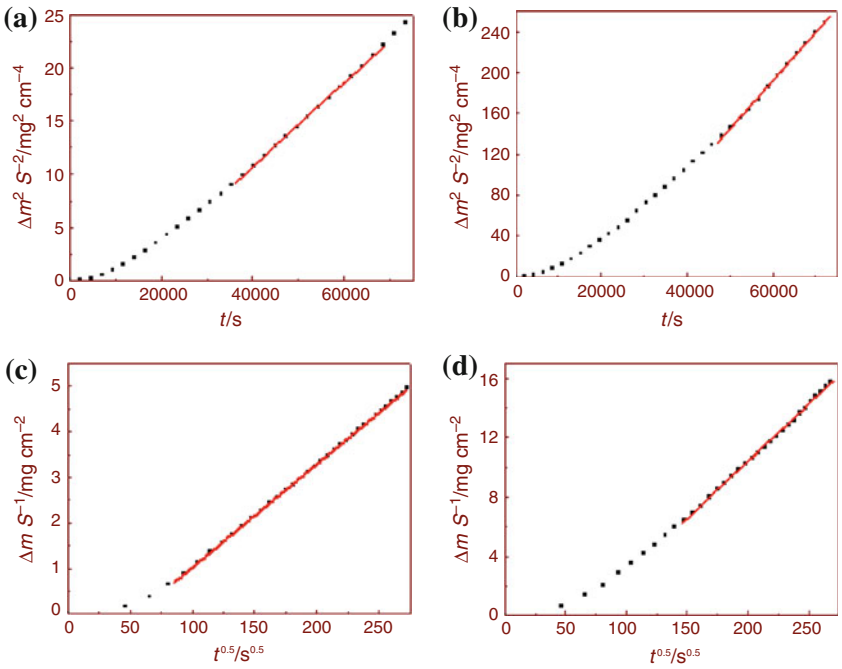

Fig. 5 Mass gain per unit area $(\Delta m/S)^2$ as a function of time during oxidation at 805 °C (**a**) and 895 °C (**b**) and the corresponding graphs (**c**, **d**) of the mass gain per unit area ($\Delta m/S$) as a function of square root of time (t)

Table 1 Calculated values of the rate constant k_p (kg^2 m^{-4} s^{-1}) at four isothermal temperatures

T/°C	$k_p/\Delta m^2\ S^{-2}\ t^{-1}$	$k_p/\Delta m\ S^{-1}\ t^{-0.5}$
805	0.39	22.65
835	1.28	40.44
865	2.43	58.04
895	4.72	76.92

The regression factors are greater than 0.999

Table 2 Calculated values of the activation energies

Equation	Activation energy E/kJ mol^{-1}	Regression factor
Δm^2 vs. t	269.5	0.995
Δm vs. $t^{0.5}$	268.5	0.993

environmental conditions of the test become significantly more intense as the temperature is increased and is in agreement with the oxidation kinetics results.

The average thickness of the scale, after 20 h of exposure at 805 °C, was measured at 46 μm (Fig. 7a). However, under the particular experimental conditions, the scale is not uniform, and its thickness varies at a range of values. This happens because high-temperature oxidation takes place through cationic migration of Fe atoms, which increases with temperature [18]. 805 °C is a low oxidation temperature, as revealed from Fig. 2, and there is restricted Fe migration, and consequently, a porous scale of low thickness is formed. At 835 °C, the thickness of the scale is approximately duplicated, and its average value was measured at 100 μm (Fig. 7b) confirming the above explanation on the mechanism of oxidation of the specimens. Therefore, in this temperature, the rate of oxidation is significantly higher than in the previous case which leads to the formation of a bigger oxide layer on surface. The oxidation mechanism is also confirmed for higher oxidation temperatures as the thickness of the scale increases further. In particular, the average thickness of the oxide scale was measured as 135 (Fig. 7c) and 185 μm (Fig. 7d) for the oxidation temperatures at 865 and 895 °C,

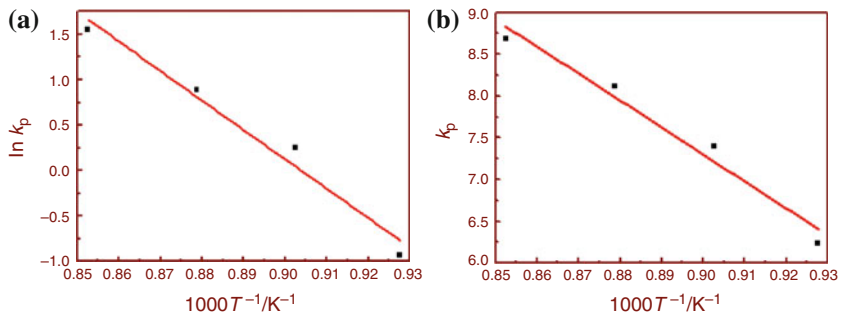

Fig. 6 Dependence of the parabolic rate constant of oxidation from the temperature using the correlations Δm^2 versus t (**a**) and Δm versus $t^{0.5}$ (**b**)

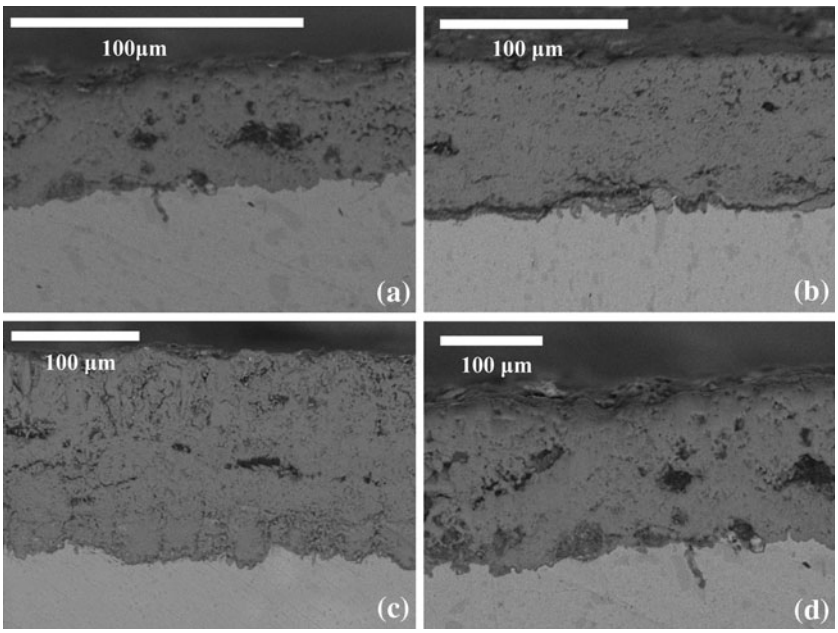

Fig. 7 Cross-sectional SEM micrographs of the specimens after isothermal oxidation at 805 °C (**a**), 835 °C (**b**), 865 °C (**c**), and 895 °C (**d**)

respectively. In the plot of Fig. 8, the thickness versus the oxidation temperature is presented. It is revealed that up to 895 °C, there is a linear dependence of the scale growth with the oxidation temperature which is described from the Eq. 3.

$$t = 1.5T - 1173 \quad (3)$$

where t (μm) is the thickness in μm, and T (°C) is the temperature.

EDX elemental analysis on the cross-sectional area of the oxidized specimens showed that the scale is composed of two different areas. In particular, of the two layers, the external layer, which is more porous and has low adherence, is composed of iron (average content 73 wt%) and oxygen (average content 27 wt%) contents. The underlying layer is much more compact and is composed also of iron and oxygen but with lower percentages (62 wt%, and 20 wt%, respectively.) and significant percentage of chromium (18 wt%) contents. These results show that the scale is composed of a mixed Fe–Cr oxide, while the outer layer is composed by Fe oxide. The low adherence of the upper oxide is due to its thermal coefficient mismatch with the underlying Fe–Cr oxide. The composition of the outer layer is also verified in the XRD patterns of all the as-oxidized specimens. The only identified phases are Fe_2O_3 and several Fe_3O_4 peaks (which are the most oxidized compounds of Fe) at $2\theta = 30.07°$, 35.419°, 43.045°, 56.924°, and 62.507°. In Fig. 9, the XRD patterns of the specimens oxidized at the lowest and the highest temperatures are presented, in which the only difference is the existence of significant higher intensity Fe_2O_3 peaks in the last case as a result of the deeper oxidation. Moreover, for the same reason, Fe_3O_4 peaks are not presented in the 895 °C graph; nor are the peaks from the underlying mixed oxides present, in either XRD patterns, because the penetration depth of the X-ray beam is not enough to traverse the whole Fe–O scale thickness.

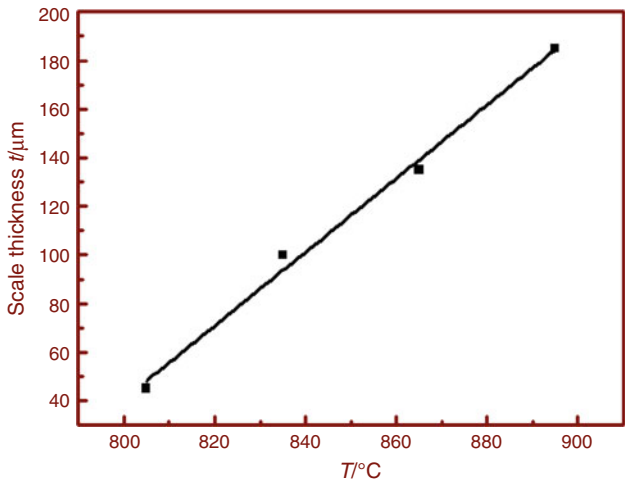

Fig. 8 Line graph of the scale thickness versus the oxidation temperature up to 895 °C

By measuring the thickness of every layer in the micrographs of Fig. 7 , it was found that, for the specimens oxidized at 805 °C, the Cr-containing layer is 10 μm, while the Fe_2O_3 layer is 36 μm. The thickness of the Cr-containing layer, for the specimens oxidized at 835 °C, is 20 μm, while the Fe_2O_3 layer is 80 μm. Finally, for the specimens oxidized at 865 and 895 °C, the Cr-containing layers are of 50 and 80 μm, while for the Fe_2O_3 layers, 85 and 105 μm, respectively. From these results, it is found that the Fe_2O_3 percentage in the scale increases in the first two cases (77% for 805 °C and 80% for 835 °C). However,

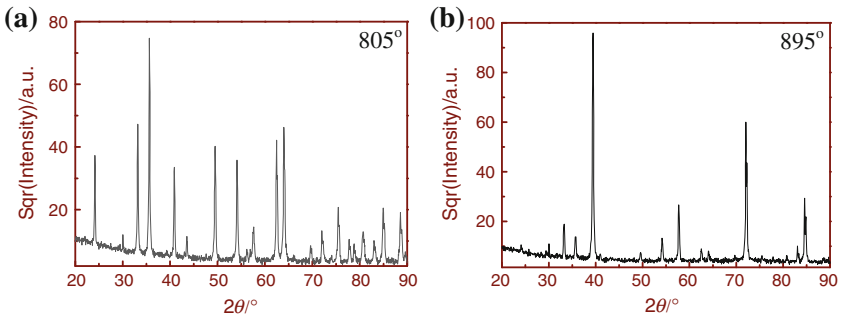

Fig. 9 XRDs of the surfaces of the tool steel specimens after thermogravimetric isothermal oxidation for 20 h at 805 and 895 °C. The indexing of the peaks was accomplished with the following PDF cards **a** 87-1164-6, 85-0987 (Fe_2O_3); **b** 79-0418 (Fe_3O_4)

this percentage decreases in the last two oxidation cases (63% for 865 °C and 57% for 895 °C). From this remark, it is concluded that the Cr oxide is primarily formed on the surface of the specimen. This layer results from the oxidation of the surface carbides which react with the atmospheric oxygen following the chemical reaction [19]:

$$2Cr_7C_3 + 27O \rightarrow 7Cr_2O_3 + 6CO \quad (4)$$

Under the effect of the high temperature, it is possible for the tool steel to undergo several structural transformations, such as the precipitation of the Cr_7C_3 in the grain boundaries of the material and dissolution [20]. Chrome, available after the dissolution of the carbides, diffuses to the external surface and reacts with oxygen forming Cr_2O_3 as the diffusion coefficient of Cr in α-Fe matrix is elevated under the particular conditions (10^{-11} cm^2 s^{-1}) [21]. Therefore, the surface becomes rich in Cr contents, which are transformed to Cr_2O_3 when reacting with the atmospheric oxygen [22]. In the next stage, the Fe cations from the substrate diffuse through the chrome oxide scale and transform it into a spinel-mixed Fe–Cr oxide, while the continuous Fe diffusion through this scale results in the formation of a Fe_2O_3 compound over the scale, as Cr cannot easily diffuse through the spinel phase [23].

The thickness of the chromite oxide increases with temperature as concluded from the experimental measurements and delays significantly the iron cations from the tool steel from reaching the surface and reacting with oxygen [24–26]. Therefore, at low temperatures (805 and 835 °C), where this oxide has lower thickness, the iron oxide scale has greater thickness as the Fe cations can traverse it easily. At higher oxidation temperatures (865 and 895 °C), where the mixed oxide layer has significantly greater thickness, it takes more time for the Fe cations to traverse it and form Fe–O compounds, which explains why its percentage was found to be lower in these cases.

The porous non-compact morphology of the Fe_2O_3 layer can be attributed to the decarburization of the tool steel. It is reported that, steels, when exposed at high temperatures, gradually lose their carbon content which diffuses to the surface [27]. Therefore, carbon comes into contact with the oxygen of the aggressive environment, which results in the evolution of gaseous CO_2 and CO. These gases create appreciable internal pressures beneath the scale, which in turns leads to the breakdown of otherwise protective scales by the formation of cracks and blisters [28]. Moreover, the appearance of several cracks can also be attributed to the misfit between the two revealed scales [29].

Conclusions

The microscopical examination of the microstructure of the tool steel showed that it is composed of chrome carbides, Cr_7C_3 and $(Cr,Fe)_7C_3$, and vanadium carbides dispersed in the ferrous matrix of the steel. The results of the different oxidation tests performed by isothermal and non-isothermal thermogravimetric tests proved that Cr–Mo–V tool steel is resistant up to 750 °C, as up to this temperature, there was no mass increase noted in the corresponding diagram. At higher temperatures (>800 °C), the oxidation rate increases, which is observed from the distinguishable change of the curve slope. The microstructural examination of the oxidized specimens showed that an oxide layer was formed in every case, which is composed of a mixed Cr–Fe oxide layer (inner layer with 62 wt% Fe, 20 wt% oxygen, and 18 wt% Cr) and the outer layer which mainly contains Fe_2O_3. Its was also found that the more the thicker is the Cr–Fe oxide inner layer the less the Fe_2O_3 compound is formed on the outer layer of the scale. Furthermore, the Fe_2O_3 layer morphology was characterized by many cracks and pores mostly attributed to the difference of thermal expansion coefficient of the as-formed oxides and the evolution of gaseous CO_2 and CO caused by the decarburization of the steel matrix. In conclusion, it can be claimed that the usage of Cr–Mo–V (Calmax) tool steel at temperatures up to 750 °C was proved to be safe as the material is fairly oxidized, while its usage at higher temperatures can provoke several microstructural transformations which can lead to an unexpected failure.

References

1. ASM International. ASM handbook. Properties and selection irons steels and high performance alloys; 1993. p. 1763.
2. Fontana MG. Corrosion engineering. 3rd ed. New York: McGraw Hill; 1986.
3. Kofstad P. High temperature corrosion. 3rd ed. New York: Elsevier; 1988.
4. Birks N, Meier GH. Introduction to high temperature oxidation of metals. London: Edward Arnold; 1983.
5. Vourlias G, Pistofidis N, Psyllaki P, Pavlidou E, Chrissafis K. Initial stages of oxidation of a precipitation-hardening (PH) steel. J Therm Anal Calorim. 2010;101:893–8.
6. Vourlias G, Pistofidis N, Pavlidou E, Chrissafis K. Oxidation behaviour of precipitation hardened steel TG, X-ray, XRD and SEM study. J Therm Anal Calorim. 2009;95:63–8.
7. Wright I. ASM handbook: vol. 13. High temperature corrosion. New York: ASM International; 1997. p. 97–101.
8. Schweitzer AP. Fundamentals of metallic corrosion. Boca Raton: CRC Press; 2007.
9. Psyllaki P, Kefalonikas G, Pantazopoulos G, Antoniou S, Sideris J. Microstructure and tribological behaviour of liquid nitrocarburised tool steels. Surf Coat Technol. 2002;162:67–78.
10. PC Powder Diffraction Files. JCPDS-ICDD; 2005.
11. Fan C, Chen MC, Chang CM, Wu W. Microstructure change caused by $(Cr,Fe)_{23}C_6$ carbides in high chromium Fe–Cr–C hardfacing alloys. Surf Coat Technol. 2006;201:908–12.
12. Detroye M, Reniers F, Buess-Herman C, Vereecken J. AES–XPS study of chromium carbides and chromium iron carbides. Appl Surf Sci. 1999;144–145:78–82.
13. Lu L, Soda H, McLean A. Microstructure and mechanical properties of Fe–Cr–C eutectic composites. Mater Sci Eng. 2003;A347:214–22.
14. ASM International. ASM handbook: vol. 13. Corrosion; 1993. p. 1286.
15. Pieraggi B. Calculations of parabolic reaction rate constants. Oxid Met. 1987;27:177–85.
16. Levy M, Farrell P, Pettit F. Oxidation of some advanced single-crystal nickel-base superalloys in air at 2000°F (1093 °C). Corrosion. 1986;42:708–13.
17. Pieraggi B, Rapp RA. Chromia scale growth in alloy oxidation and the reactive element effect. J Electrochem Soc. 1993;140:2844–50.
18. Vourlias G, Chaliampalias D, Zorba TT, Pavlidou E, Psyllaki P, Paraskevopoulos KM, Stergioudis G, Chrissafis K. A combined study of the oxidation mechanism and resistance of AISI D6 steel exposed at high temperature environments. Appl Surf Sci. 2011;257(15):6687–98.
19. Malik AU. High-temperature oxidation of transition metal, carbide-dispersed iron-base alloys. Oxid Met. 1985;24(5–6):233–63.
20. Durham RN, Gleeson B, Young DJ. Factors affecting chromium carbide precipitate dissolution during alloy oxidation. Oxid Met. 1998;50:139–65.
21. Smithells CJ. Metals reference book, vol. II. London: Butterworths; 1967. p. 664.
22. Riffard F, Buscail H, Caudron E, Cueff R, Issartel C, Perrier S. In-situ characterization of the oxide scale formed on yttrium-coated 304 stainless steel at 1000 °C. Mater Charact. 2002;49:55–65.
23. Robertson J. Control of oxygen concentration in liquid lead and lead bismuth. Corros Sci. 1989;29:1275–85.
24. Stringer J. Reactive element effect in high-temperature corrosion. Mater Sci Eng. 1989;A120:129–37.
25. Cotell CM, Yurek GJ, Hussey RJ, Mitchell DF, Graham MJ. The influence of grain-boundary segregation of Y in Cr_2O_3 on the oxidation of Cr metal. Oxid Met. 1990;34:173–200.
26. Ecer GM, Singh RB, Meier GH. The influence of superficially applied oxide powders on the high-temperature oxidation behaviour of Cr_2O_3-forming alloys. Oxid Met. 1982;18:55–81.
27. Caplan D, Sproule GI, Hussey RJ, Graham MJ. Oxidation of Fe–C alloys at 700 °C. Oxid Met. 1979;13:255–72.
28. Malik AU, Whittle DP. Oxidation of Fe–C alloys in the temperature range 600–850 °C. Oxid Met. 1981;16(5–6):339–53.
29. Hirth JP, Pieraggi B, Rapp RA. The role of interface dislocations and ledges as sources/sinks for point defects in scaling reactions. Acta Metall Mater. 1995;43:1065–73.